Robotica (2007) volume 25, pp. 375–383. © 2007 Cambridge University Press
doi:10.1017/S0263574706003195 Printed in the United Kingdom

Development of an image-guided robotic system for surgical positioning and drilling

Ching-Shiow Tseng†, Chiao-Chi Huang‡ and Chen-San Chen*

†*Institute of Biomedical Engineering, National Central University, Chungli 320, Taiwan*
‡*Department of Mechanical Engineering, National Central University, Chungli 320, Taiwan*
**Department of Mechanical Engineering, Northern Taiwan Institute of Science and Technology, Taipei 112, Taiwan*

(Received in Final Form: November 14, 2006. First published online: January 18, 2007)

Abstract
This study develops a novel image-guided robotic system that can be used to position biopsy needles or drill fixation holes. After the patient has received a CT-scan, the registration of the image, localizer (patient), and robot frames will be done by finding the optimum transformation matrix among the image and localizer coordinates of the fiducial markers and the DRFs mounted on the robot. Then, surgical paths planned on the computer displayed images can be transformed to the robot frame, and the robot is thus capable to move surgical tools to the preplanned location. The positioning error is about 2 mm and the orientation error is about 0.23°.

1. Introduction

Surgical planning and navigation systems can help surgeons to preplan treatment procedures with computers. However, due to the precision limitations of unguided handheld tools and the lack of direct visual guidance to the target, surgeons generally cannot fulfill the preoperative planning precisely during surgery. Current treatment methods do not easily meet spatial and stable positioning requirements. However, robotic technology has been successfully introduced and applied to computer-assisted surgery during the last decade.[19]

The pioneers in the use of general-purpose robots for surgery were Kwoh *et al.*,[2] who used a six-axis industrial robot to replace the stereotactic frame for the guidance of biopsy needles in neurosurgery. Another system for percutaneous biopsies (e.g., the kidney) was developed by Potamianos *et al.*[3] The system displayed a computer-generated model of a biopsy needle superimposed on the static fluoroscopic images of the patient, as the real needle was manually moved about.

Biopsy is often performed to diagnose diseases and lesions. Most current needle biopsy procedures have to be performed under empiric protocols, leading to unsatisfied detection rates. Usually, biopsy procedures are performed by a radiologist under the guidance of ultrasound or CT scan. But it is hard to figure out the actual position of the target and the optimal insertion direction only by two-dimensional (2-D) images. Cleary *et al.* [20,21] have been using C-arm and CT for robotic biopsy. On the other hand, bone drilling is one of the important procedures in orthopedic surgery.[16–18] Currently, drilling procedure is carried out by surgeons themselves under the assistance of fluoroscopic images, which does not promise accurate positioning. Also, the accumulation of X-ray dose poses high risk to the surgeons' health.

There are several groups who adopted different approaches to the robotic orthopedic surgery.[4–8] Conventional total knee replacement (TKR) surgery requires the repeated use of a series of jigs and fixtures. It is possible to accumulate positioning errors in cutting planes. Lea *et al.*[4] proposed a system that used calibrated industrial robot to perform TKR surgery. Davies *et al.*[9] used an interactively controllable robot to perform TKR surgery. The robot arm was force-controlled and could be moved by the surgeon manually to the cutting position. The motion of the cutter was restricted by decreasing controller gains near the boundary of the preset working space.

Several surgical auxiliary robotic devices have been designed to meet the requirement of spatial positioning accuracy[7,10,11,22,23] (like the use of serial jigs in TKR surgery,[9] C-arm in orthopedic surgery, and stereotactic frame in brain biopsy).[1,12,13] But the inconvenience and limited applicability of these devices have led many researchers to explore the potential of using robotic devices to augment a surgeon's ability to perform geometrically precise, dexterous, and steady tasks planned from CT or other images. Brief *et al.*[14] presented an image-guided robotic system in the applications of bone drilling and insertion of dental implants. The robot was calibrated to have a positioning accuracy better than 0.03 mm; the overall positioning error of this system is about 1 mm. Lueth *et al.*[11,15] presented an application in maxillofacial surgery. They intended to use a robot as an intelligent instrument for handling various kinds of surgical tools (like electric drill, taper, screwdriver, electric saw, retractor hook), and for the guidance of accurate implants placement. The robot is interactively planned and controlled to handle the medical instruments only within a predefined restricted workspace. Santos-Munné *et al.*[8] described a robotic system for pedicle screw placement. He used A/P and sagittal fluoroscopic images of the vertebra and the array of fiducial spheres on the end-effector to establish intraoperative relation between the robot and the vertebra.

The objective of this research is to develop an image-guided robotic system to provide surgeons with benefits. The system integrates advanced image processing and computer graphics techniques with a robot and a three-dimensional (3-D) optical localizer, to achieve effective surgical planning,

*Corresponding author. E-mail: cstseng@cc.ncu.edu.tw

https://doi.org/10.1017/S0263574706003195 Published online by Cambridge University Press

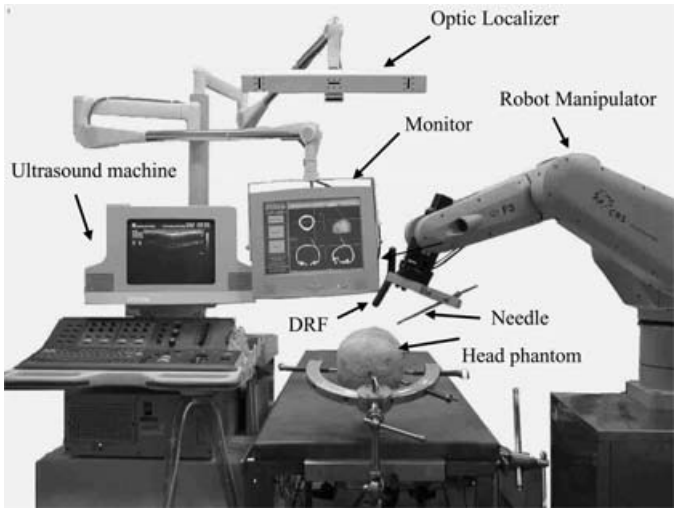


Fig. 1. SPANS robotic system.

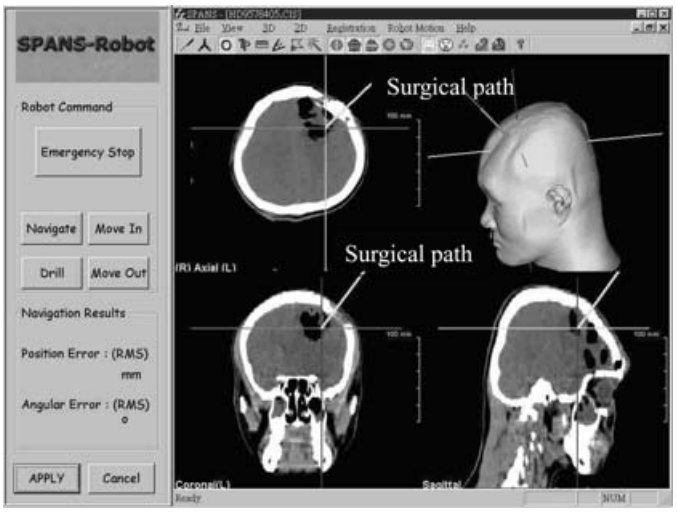


Fig. 2. Screenshot of the GUI of the SPANS robotic system.

more accurate outcome, and autonomous execution of surgical interventions (under the supervision of the surgeon).

2. System Overview

Figure 1 shows the developed image-guided robotic system with an ultrasound machine, which is used for detecting shifted brain tumor intraoperatively. The hardware of the image-guided robotic system is composed of three parts:

1. A personal computer running Windows XP that integrates all system software including graphics-based planning software for preplanning the paths of surgical tools to the desired lesions, robot motion software for transforming surgical tool paths into robot paths, and robot communication software for commanding the robot to move surgical tools to the planned paths.
2. A 3-D optical localizer (Flash Point Model 5000 with an accuracy of 0.3 mm for each LED, produced by Image Guided Technologies, Inc.) that tracks the positions of the dynamic reference frames (DRFs) mounted onto the robot manipulator and surgical tools. In other words, it tracks the positions and orientations of the robot manipulator and surgical tools in almost real time. Each DRF has at least three inferred LEDs whose light spots are detected by the three linear cameras of the localizer, and are used to calculate the spatial positions of the LEDs (three nonlinear LEDs determine a spatial plane or a spatial frame).
3. A six-degree-of-freedom CRS robot manipulator that moves the surgical tools to the preplanned paths under the guidance of the optical localizer.

The image sources used in this system can be ultrasound (US), computed tomography (CT), or magnetic resonance imaging (MRI) images. US is movable and convenient for soft tissue detection, but image quality is not as good as CT or MRI. CT is generally used for prime tomography of hard and soft tissues, while MRI is better for soft tissue tomography (it has a better contrast of soft tissues than CT). All of the three image modalities are 2-D. It is recommended to reconstruct the images into 3-D models for better diagnosis by using reconstruction algorithms (e.g., Marching Cube Algorithm).

Except reconstructed 3-D models, three orthogonal section images (axial, sagittal, and coronal views) can also be generated from the original images as shown in Fig. 2. Surgeons can preplan optimum surgical paths on any two of the three orthogonal images by translating and rotating the path segments (the surgical paths of Fig. 2) to the target lesions (the black areas in the images). Whenever the surgical path is moved, the computer will automatically generate and display new orthogonal section images, which pass through the end point of the path (the intersection of the cross in Fig. 2). This real-time image display will facilitate the diagnosis and treatment planning of lesions.

After the surgical path has been planned, the location of the path relative to the image frame will be transformed relative to the localizer frame and then to the robot frame through frame registration among the three frames as described below. Therefore, under the guidance of the optic tracker, the robot manipulator will be able to move the surgical tool to the planned location.

3. Image-Guided Robotic Navigation

The operative flow of the system is shown in Fig. 3. The main topics to be solved are the registration among the image, localizer, and robot frames, and calibration between the DRF frame and tool tip frame of the robot. Registration is the determination of the spatial relationships among the coordinate frames. When the registration has been completed, a designated path of surgical tool planned on the computer display can be transformed to the robot frame through the localizer frame. The path relative to the robot frame will be converted into a set of corresponding robot joint angles, which will enable the robot to bring the surgical tool, such as a pneumatic drill, to follow the preplanned path and reach the target lesion of the patient. For some reasons, if the surgical tool does not reach the target precisely enough, fine position/orientation tuning of the robot manipulator will be done to compensate the error.

https://doi.org/10.1017/S0263574706003195 Published online by Cambridge University Press

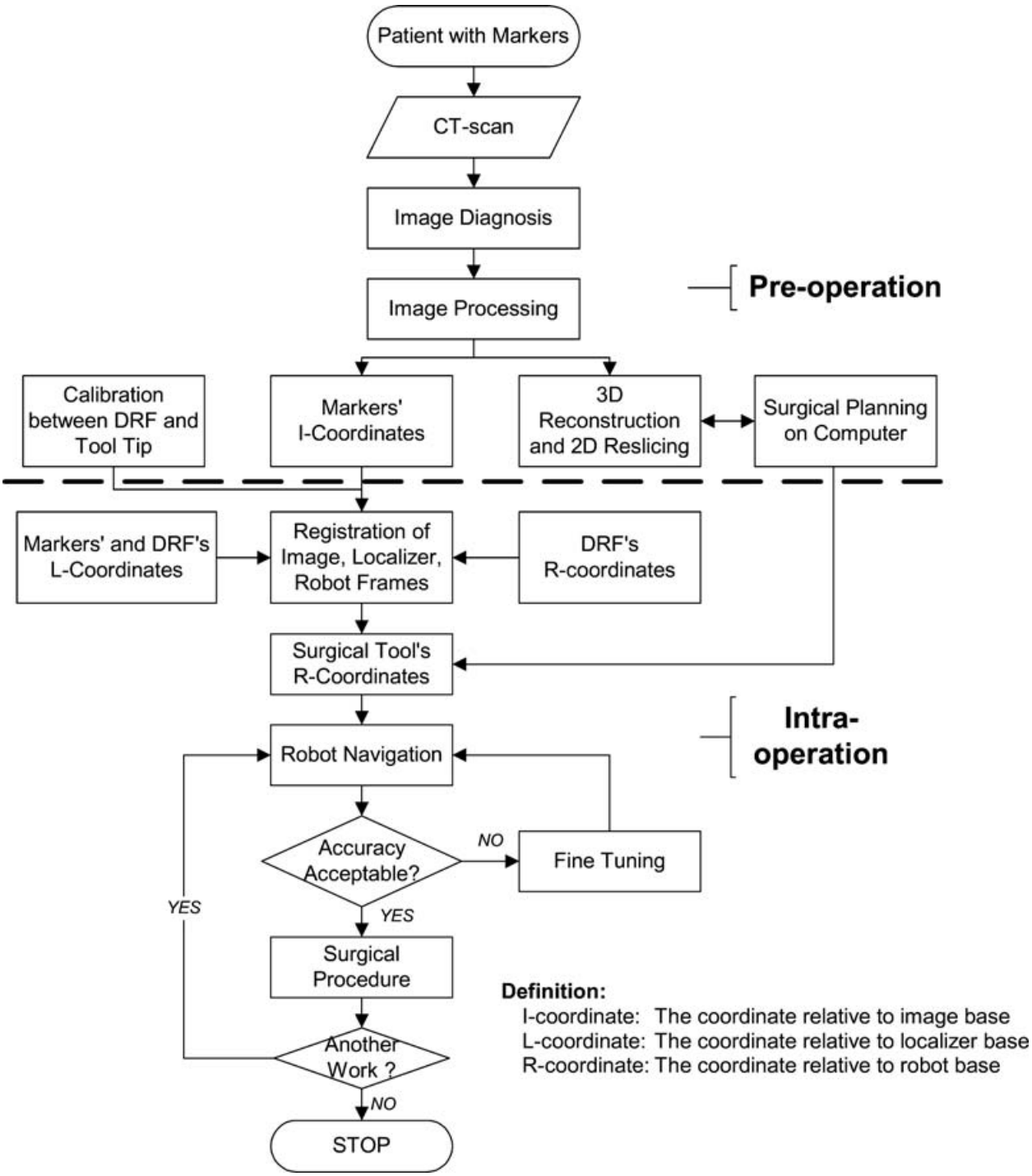


Fig. 3. Operative flowchart of the SPANS-Robot system.

3.1. Registration between the image and patient (localizer) frames

The registration between the patient's images and the patient is to establish their spatial relationship that can be utilized to apply the preoperation planning to the actual patient. First, fiducial markers, which are clearly distinguishable on the images, are attached to the pertinent anatomical structure of the patient prior to imaging. Registration is done by finding the spatial transformation matrix between the image coordinates and the localizer coordinates of the markers, in which the latter is measured during surgery by the optical localizer.

There are six unknowns in transformation matrix ${}^{I}_{L}T$ between the localizer and image frames. Since the mapping among the image and localizer coordinates of the markers are quite uncertain, optimization algorithms such as least square algorithm or genetic algorithm will be applied to find the optimum solution of the six unknowns. Here, genetic algorithm is introduced to find the optimal transformation matrix ${}^{I}_{L}T$. The disparity function D is defined as

$$D = \sum_{i=1}^{n} \left[\text{dist}({}^{I}P_i, {}^{I}P'_i)\right]^2 = \sum_{i=1}^{n} \left[\text{dist}\left({}^{I}P_i, {}^{I}_{L}T\,{}^{L}P_i\right)\right]^2 \qquad (1)$$

https://doi.org/10.1017/S0263574706003195 Published online by Cambridge University Press

where

dist(x, y): The distance between the two positions x and y.
${}^{I}P_i$, ${}^{L}P_i$: The ith marker's image and localizer coordinates, respectively.
${}^{I}P'_i$: The transformed image coordinates of the ith marker.
n: The number of fiducial markers.

Another DRF is fixed on the patient's pertinent anatomy structure, which has a fixed spatial transformation with the patient, and it is used for the real-time tracking of the actual location of the patient for registration compensation.

3.2. Calibration between the DRF and the robot's tool tip

A major issue for an image-guided robotic system is to ensure that the robot positioning is accurate. Most industrial robots are built with high repeatability but insufficient positioning accuracy. Many factors may lead to robot's positioning error, such as environment, robot parameters, sensors, computing error, and payload. Robot calibration requires significant effort. Instead of proceeding with robot calibration, an offset calibration technique is proposed here.

The offset calibration between the tool tip frame and the DRF frame mounted on the end effector of the robot is to find the transformation matrix ${}^{\text{DRF}}_{\text{Tip}}T$, which is a fixed matrix. Then, the position of the tool tip relative to the optical localizer will be determined through the frame of the DRF. The 4×4 matrix ${}^{\text{DRF}}_{\text{Tip}}T$ has the following general form

$$ {}^{\text{DRF}}_{\text{Tip}}T = \begin{bmatrix} R & P \\ 0 & 1 \end{bmatrix}. \tag{2} $$

The "R" term is a 3×3 orientation matrix composed of the direction cosines of the surgical tool tip frame with respect to the DRF frame, which can also be represented by the Euler angles (α, β, γ). The "P " is a 3×1 position vector from the center of the DRF frame to the tip of the surgical tool. Once the matrix ${}^{\text{DRF}}_{\text{Tip}}T$ is determined, the surgical tool tip frame relative to the DRF frame can be determined as

$$ {}^{L}_{\text{Tip}}T = {}^{L}_{\text{DRF}}T \times {}^{\text{DRF}}_{\text{Tip}}T. \tag{3} $$

3.2.1. Calibration of positional offset. The DRF frame is defined by the positions of three LEDs on the DRF, as shown in Fig. 4. The tool tip frame is defined at the tip of the tool, whose Z-axis is coaxial with the tool axis of the surgical tool. The offset between the DRF frame and tool tip frame is calibrated by rotating the surgical tool about a fixed point for more than three orientations, and by recording the position and orientation of the DRF frame at these poses (Fig. 5). Since the tool tip always points to a fixed point, the calculated tip position from different poses of the DRF should be the same, which is

$$ {}^{L}_{\text{Tip}}P_i = {}^{L}_{\text{DRF}}T_i \times {}^{\text{DRF}}_{\text{Tip}}P, \qquad i = 1, 2, \ldots, n \tag{4} $$

where ${}^{L}_{\text{Tip}}P_i$ is the calculated tip position, ${}^{L}_{\text{DRF}}T_i$ is the position and orientation of the DRF frame relative to the localizer

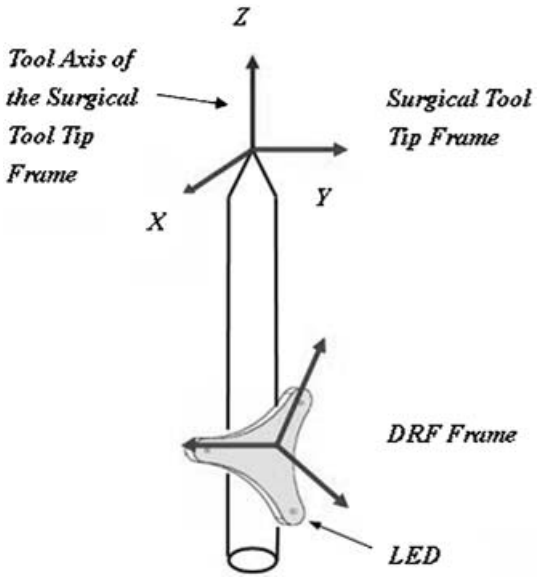


Fig. 4. Defined surgical tool tip frame and the DRF frame.

frame, ${}^{\text{DRF}}_{\text{Tip}}P$ is the linear offset between the surgical tool tip, relative to the DRF frame, and n is the number of the DRF frames recorded.

We use Genetic Algorithm again to find the optimal solution of the offset. The disparity function D is defined as

$$ D = \sum_{i=1}^{n} \left[\text{dist}\left({}^{L}_{\text{Tip}}P_i, {}^{L}_{\text{Tip}}\overline{P} \right) \right]^2, \tag{5} $$

where

$$ {}^{L}_{\text{Tip}}\overline{P} = \frac{\sum_{i=1}^{n} {}^{L}_{\text{Tip}}P_i}{n}, $$

3.2.2. Calibration of angular offset. For the measurement of the angular offset, a laser pointer is used as the angular calibration device. The laser pointer is mounted on the robot end effector, and its optical axis is coaxial with the symmetrical axis of the surgical tool. Therefore, by the linearity of the laser, the laser beam will direct the orientation of the tool axis of the tool tip frame.

If the angular offset of ${}^{\text{DRF}}_{\text{Tip}}T$ (the "R" component of Eq. 2) is well calibrated, the spot shot of the laser pointer should always be located at the same position when the tool is moved along the tool axis, as illustrated in Fig. 6. If the spot changes positions while the laser pointer moves along the tool axis, then the angular offset has to be revised.

The initial angular offset is set by the geometric relation; however, due to the imprecision of the mechanical setup, the actual angular offset has to be determined for higher accuracy. As shown in Fig. 7, the modified yaw and pitch angles can be approximately calculated by applying trigonometric method of displacement of the laser spots on X and Y axes of the tool tip frame and the distance of the laser pointer tip to the laser spot, as

https://doi.org/10.1017/S0263574706003195 Published online by Cambridge University Press

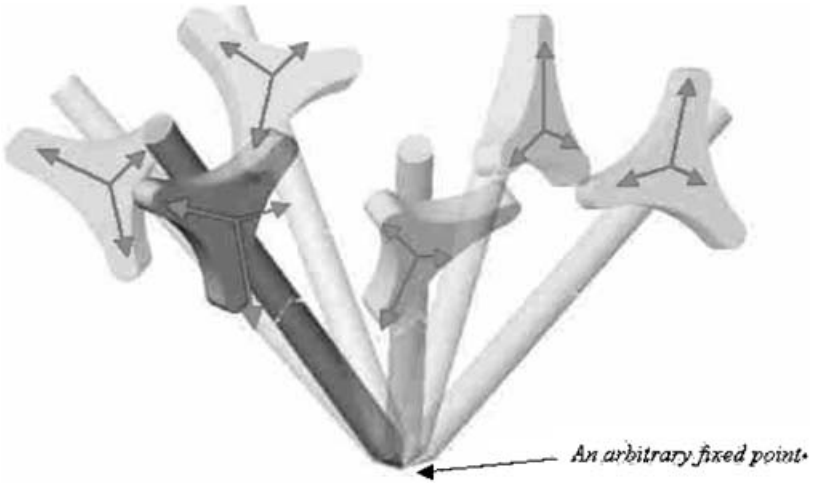


Fig. 5. Tool tip rotates about an arbitrary fixed point.

$$\Delta\alpha = \frac{d_x}{L}, \qquad \Delta\beta = \frac{d_y}{L}. \tag{6}$$

3.3. Registration between the localizer and robot frames

Once the patient and image frames are registered as described above, the surgical path planned on the images can be transformed relative to the localizer frame, which indicates the actual position and orientation of the surgical path on the patient. Moreover, the surgical path relative to the robot frame will be calculated, if the robot tool frame has been registered with the localizer frame. Then the robot will be able to move the surgical tool to the planned path.

The geometric relation between the surgical tool tip mounted on the robot and the robot base is defined as ${}^{R}_{\mathrm{TIP}}T$, which is calculated from the geometric transformation (forward solution) of the robot. The transformation matrix between the localizer and the robot frame ${}^{R}_{L}T$ can be obtained by

$${}^{R}_{L}T = {}^{R}_{\mathrm{TIP}}T \times {}^{\mathrm{TIP}}_{\mathrm{DRF}}T \times {}^{\mathrm{DRF}}_{L}T \tag{7}$$

where ${}^{\mathrm{TIP}}_{\mathrm{DRF}}T$ is the transformation between the DRF and the surgical tool tip, and ${}^{\mathrm{DRF}}_{L}T$ is the transformation of the DRF frame to the localizer's frame.

Through Eq. (7), the target location of the tool tip relative to the localizer frame can be transformed to the robot frame as

$${}^{R}_{\mathrm{Tip}}T = {}^{R}_{L}T \times {}^{L}_{\mathrm{Tip}}T \tag{8}$$

where ${}^{L}_{\mathrm{Tip}}T$ is the target tool tip location, ${}^{R}_{L}T$ is the transformation of the localizer relative to robot frame, and ${}^{R}_{\mathrm{Tip}}T$ is the target location of the tool tip relative to the robot frame.

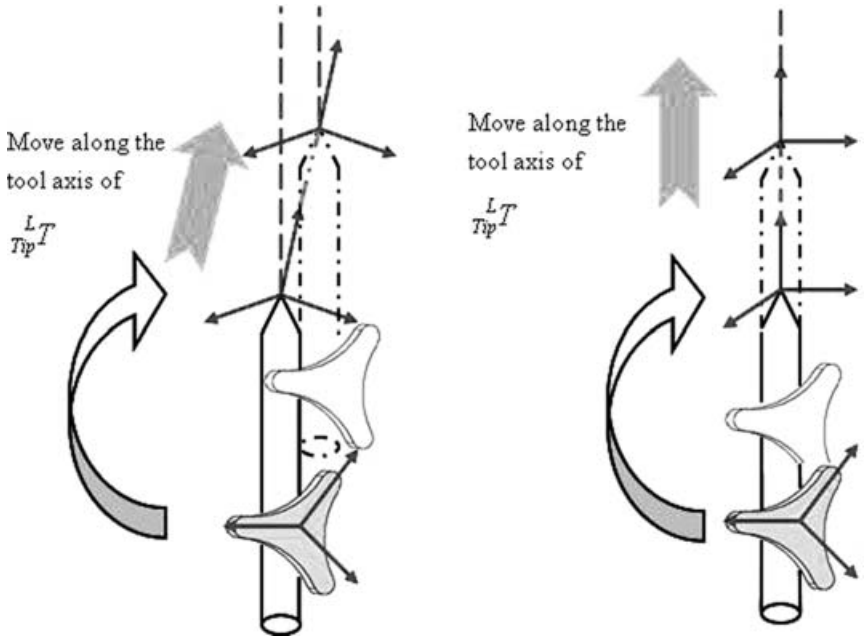


Fig. 6. Illustration of the verification of angular offset.

https://doi.org/10.1017/S0263574706003195 Published online by Cambridge University Press

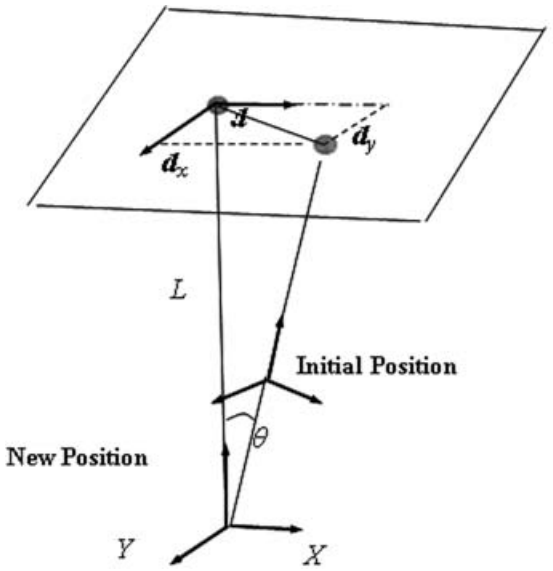


Fig. 7. Laser spot moves while the laser moves along the surgical tool tip frame.

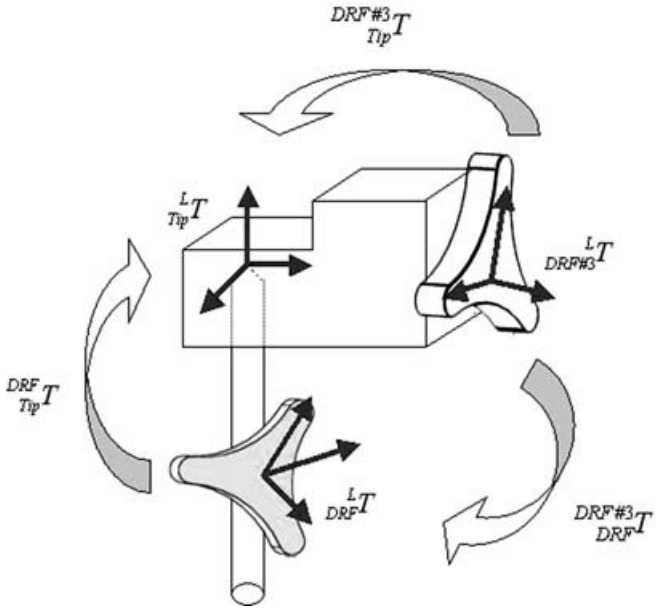


Fig. 8. Use of the calibration block.

3.4. *Fine-tuning approach*

As we already know, the robot has excellent repeatability but poor positioning accuracy. Hence fine-tuning of the robot movement will be necessary to compensate positioning error, which is affected by the measuring accuracy of the localizer and the transformation matrix ${}^{\text{DRF}}_{\text{TIP}}T$.

The fine-tuning approach is dependent on the difference between the measured tool tip location ${}^{L}_{\text{Tip}}T_{\text{Measured}}$ and planned tool tip location ${}^{L}_{\text{Tip}}T_{\text{Planned}}$. If the position and orientation errors are less than the rated accuracy specification of the localizer, no fine-tuning procedure will be executed. Whereas, if the errors are greater than the localizer accuracy and desired positioning accuracy, both the measured and planned tip locations relative to the localizer frame will be transformed to those relative to the robot frame, that is ${}^{R}_{\text{Tip}}T_{\text{Measured}}$ and ${}^{R}_{\text{Tip}}T_{\text{Planned}}$. Then the robot is commanded to compensate the positioning difference between them, which can be transformed to joint angles. The procedure is repeated until the desired positioning accuracy is reached.

4. Calibration Block

From previous descriptions, we know that the calibrated offset between the DRF and the surgical tool tip ${}^{\text{DRF}}_{\text{Tip}}T$, is one of the most important factors affecting the positioning accuracy of the system. For practical applications, efficient and correct determination of the elements of ${}^{\text{DRF}}_{\text{Tip}}T$ is important because different surgical tools will need new calibration. To solve the problem, a calibration block is introduced to rapidly obtain the correct transformation matrix ${}^{\text{DRF}}_{\text{Tip}}T$. The calibration block is designed with holes of specific diameters that fit different sizes of surgical tools, and a fixed $\text{DRF}_{\#3}$ mounted on it for location tracking.

The relation among the surgical tool tip frame ${}^{L}_{\text{Tip}}T$, the DRF frame ${}^{\text{L}}_{\text{DRF}}T$, and the DRF3 frame ${}^{L}_{\text{DRF\#3}}T$ relative to the localizer is illustrated in Fig. 8. The calibration parameter of the block ${}^{\text{DRF\#3}}_{\text{Tip}}T$ is a fixed transformation matrix because of the geometrical unity of the block.

To determine the transformation matrix ${}^{\text{DRF\#3}}_{\text{Tip}}T$, the transformation ${}^{\text{DRF}}_{\text{Tip}}T$ is first solved by the same method described in Section 3.2. Then the surgical tool is inserted into the block, and the transformation ${}^{\text{DRF\#3}}_{\text{DRF}}T$ can be calculated from the sequential matrix multiplication from the DRF#3 and DRF frame as

$$ {}^{\text{DRF\#3}}_{\text{Tip}}T = {}^{\text{DRF\#3}}_{\text{DRF}}T \times {}^{\text{DRF}}_{\text{Tip}}T \tag{9} $$

where

$$ {}^{\text{DRF\#3}}_{\text{DRF}}T = {}^{\text{DRF\#3}}_{L}T \times {}^{L}_{\text{DRF}}T. $$

Once the surgical tool is changed, ${}^{\text{DRF}}_{\text{Tip}}T$ will be altered. Nevertheless, it can be calculated rapidly through dynamically measured ${}^{\text{DRF}}_{\text{DRF\#3}}T$ and the offline measured ${}^{\text{DRF\#3}}_{\text{Tip}}T$ as

$$ {}^{\text{DRF}}_{\text{Tip}}T = {}^{\text{DRF}}_{\text{DRF\#3}}T \times {}^{\text{DRF\#3}}_{\text{Tip}}T. \tag{10} $$

5. Experiment Results and Discussion

5.1. *Accuracy of robot positioning after calibration*

To evaluate the positioning accuracy of the robot after calibration, 10 spatial points (the fiducial markers on the skull, see Fig. 9) are given as the targets for the surgical tool tip. The positions of target points are measured by the optical localizer, and the robot is then commanded to move the surgical tool to reach them. The positioning error is the distance between the target point and tool tip. The angular error is obtained by mounting a laser pointer on the robot, where the laser light is coaxial to the surgical tool axis. Then the robot is commanded to move a distance along the surgical

https://doi.org/10.1017/S0263574706003195 Published online by Cambridge University Press

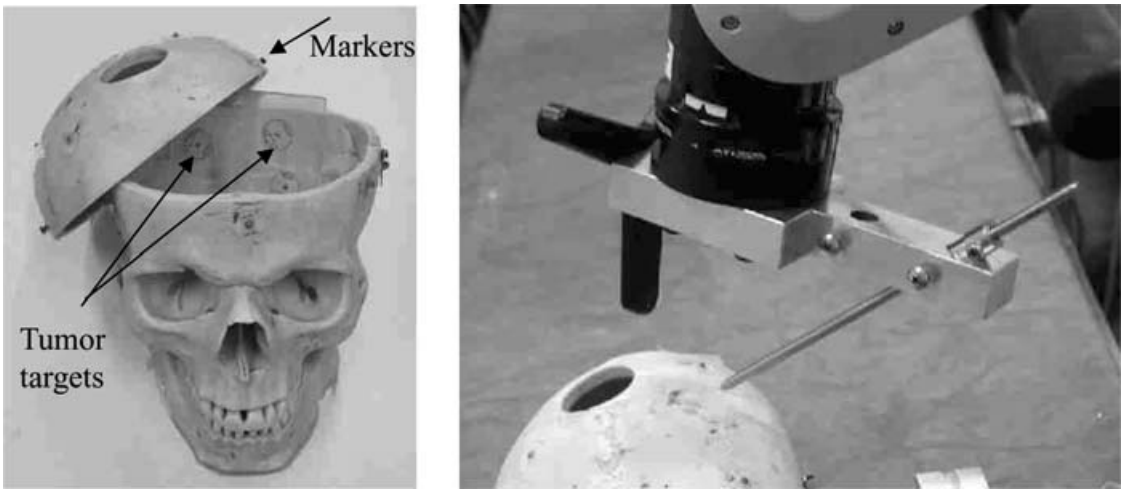


Fig. 9. Skull phantom and robot positioning.

Table I. Positioning errors of the robot tool tip.

No.	Positioning error (mm)	Angular error (°)
1	0.5	0.29
2	1.1	0.20
3	0.6	0.14
4	0.6	0.15
5	0.8	0.23
6	1.2	0.29
7	0.7	0.16
8	1.0	0.17
9	0.8	0.29
10	1.0	0.14
Mean	0.83	0.21
Std. Dev.	0.235	0.064

tool axis. The approximate angular error is calculated by dividing the distance between the two laser spots (d) by the distance the laser pointer (L) moved.

The results of Table I show that the average positioning error is 0.83 mm and angular error is 0.21°. The positioning accuracy is suitable for the application of robotic biopsy of tumor as shown on the right of Fig. 9.

5.2. Image-guided robotic navigation

In Fig. 9, 10 fiducial markers are stuck on the skull phantom and four fiducial markers stuck on the acrylic board within the skull are given as the tumor targets. Then the skull received a CT-scan with 1 mm thickness, 512 × 512 pixel resolution, and 200 mm × 200 mm scanning field. Therefore, each of the image voxels is 0.391 mm × 0.391 mm × 1 mm in dimension.

The image and localizer coordinates of the 10 markers are first calculated and measured respectively to perform the registration between the image frame and the localizer frame. The surgical tool paths pointing to the tumor targets are then planned on the computer-displayed image. Then the robot is commanded to align the surgical tool to the planned surgical tool path and to reach the tumor targets.

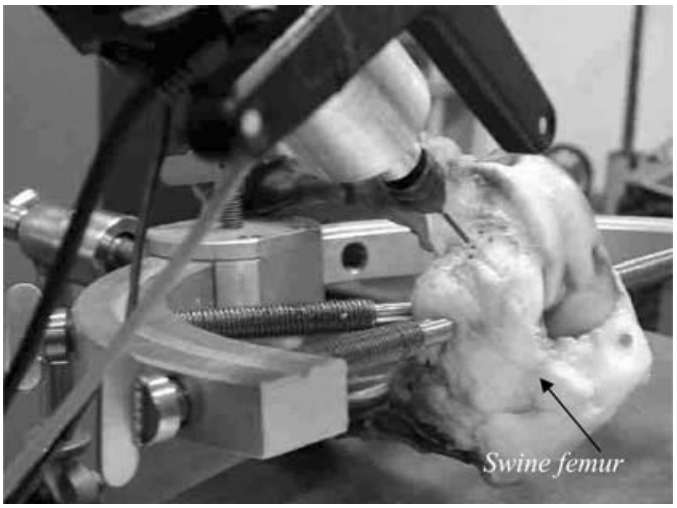


Fig. 10. Drilling experiment of a swine femur block.

Table II. Errors of tumor target positioning.

No.	Positioning error (mm)	Angular error (°)
1	2.0	0.28
2	1.6	0.19
3	1.8	0.16
4	2.1	0.29
Mean	1.9	0.23

The experimental results of Table II indicate that positioning errors of tumor target are greater than those of the positioning errors of the robot tool tip shown in Table I. The reasons of increased errors include the CT image resolution, localizer's accuracy, registration between the image and localizer frames, accuracy of the calibrated robot, and the accuracy of image coordinates of tumor targets. The data of Table II indicate that this system can locate tumor targets with a size of above 2.0 mm.[3]

5.3. Image-guided robotic drilling experiment

The tool chosen for drilling is a 2 mm twisted electric drill with two flutes and two cutting edges, 120° point angle, and

https://doi.org/10.1017/S0263574706003195 Published online by Cambridge University Press

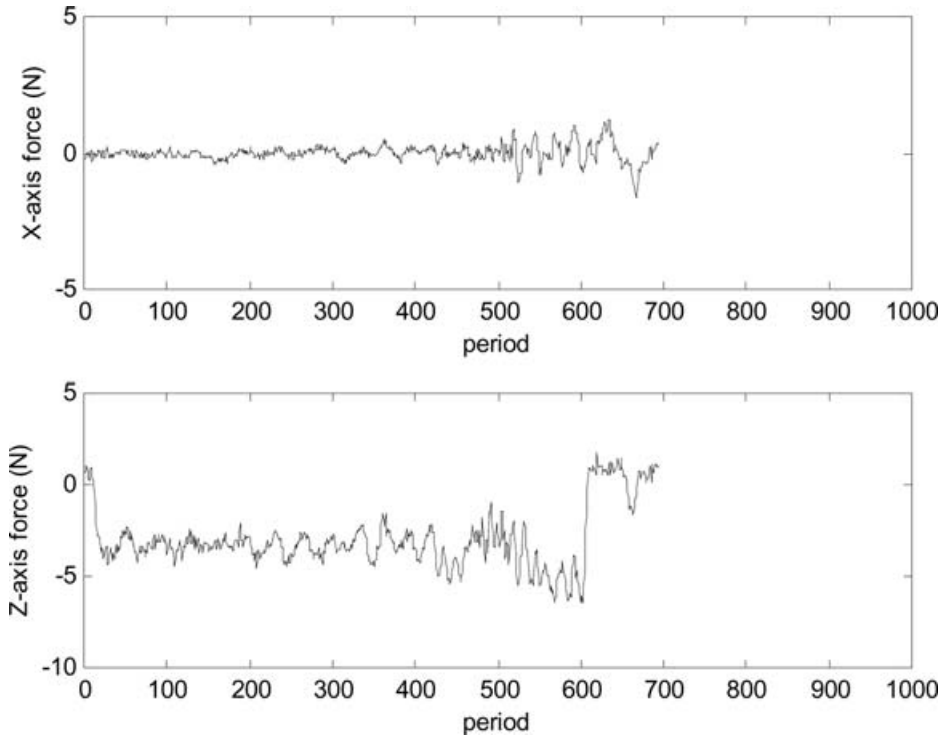


Fig. 11. Force profiles of the swine femur drilling experiment.

about 25° helix angle. The maximum rotational speed of the electric drill can reach upto 20,000 rpm.

A swine femur block is selected as the test piece. The test piece is fixed with clamps mounted on the OR table as shown in Fig. 10. The experiment is for characterizing the drilling force during the drilling process through the real bone.

The robot used is the six-axis CRS F3 robot with force control. Force control is adapted for robotic drilling procedure in this system. The drilling depth is set to be 15 mm, which is monitored by the optical localizer. Once the drill depth is reached, the robot is commanded to stop and exert no thrust force. The experimental result is shown in Fig. 11.

The return to zero force at period 600 indicates that the drilling is completed due to no drilling force along *Z*-axis. Although the force control performance is affected by the noise generated by the rotating drill, the overall robotic drilling performance remains satisfactory.

6. Conclusion

This study presents an image-guided robotic navigation system for surgery. This system enables the surgeon to diagnose and plan tool paths on computer-displayed images. Under the guidance of an optical localizer, the robot can move surgical tools to the planned target locations automatically. The accuracy of this image-guided robotic system enables the biopsy of small and deep-seated lesions, and minimizes the necessity of trial and error, thus reducing the harm to the patient. It is highly promising as a standard surgical assistance device in the near future.

Acknowledgment

This work was supported by the National Science Council, Taiwan, under the contract of NSC 94-2213-E-008-039 and Veterans General Hospital–University System of Taiwan Research Grant under contract TVGH-UST 95-G4-04-02.

References

1. Y. S. Kwoh, J. Hou, E. A. Jonckheere and S. Hayati, "A robot with improved absolute positioning accuracy for CT guided stereotactic brain surgery," *IEEE Trans. Biomed. Eng.* **35**(2), 153–160 (Feb. 1988).
2. Y. S. Kwoh, I. S. Reed, J. S. Chen, H. M. Shao, T. K. Truong and E. Jonckheere, "A new computerized tomography-aided robotic stereotaxis system," *Robot. Age*, 17–22 (Jun. 1985).
3. P. Potamianos, B. L. Davies and R. D. Hibbert, "Intra-operative imaging guidance for keyhole surgery," *Proceedings of International Symposium on Medical Robotics and Computer Assisted Surgery*, Pittsburgh, PA **1**, (1994) pp. 98–105.
4. J. T. Lea, D. Watkins, T. C. III Kienzle, A. Mills, M. A. Peshkin and S. D. Stulberg, "Registration and immobilization for robot-assisted orthopedic surgery," *Proceedings of International Symposium on Medical Robotics and Computer Assisted Surgery*, Pittsburgh, Pennsylvania, USA (1994) pp. 63–68.
5. J. Troccaz, S. Lavallée, P. Sautot, P. Cinquin, B. Mazier and J. P. Chirossel, "Robot assisted spine surgery," *Medi-Mechatronics Workshop*, Málaga, Spain (Oct. 1992).
6. T. C. Kienzle, S. D. Stulberg, M. Peshkin, A. Quaid and C. Wu, "An integrated CAD-Robotics System for total knee replacement," *Surgery Proceedings of IEEE International Conference on Robotics and Automation*, Atlanta, GA (1993) pp. 99–894.
7. F. A. III Matsen, J. L. Garbini, J. A. Sidles, B. Pratt and D. Baumgarten, "Robotic assistance in orthopedic surgery," *Clin. Orthop.* **296**, 178–186 (1993).

https://doi.org/10.1017/S0263574706003195 Published online by Cambridge University Press

8. J. J. Santos-Munné, M. A. Peshkin, S. Mirkovic, S. D. Stulberg and T. C. Kienzle, "A stereotactic/robotic system for pedicle screw placement," *Proceedings of Medicine Meets Virtual Reality III* San Diego, CA (1995) pp. 326–333.
9. B. L. Davies, W. J. Lin, R. D. Hibberd and J. C. Cobb, "Active compliance in robotic surgery—The use of force control as a dynamic constraint," *J. Eng. Med.* (4), 285–292 (Sep. 1997).
10. D. H. Robert and Y. Matsuoka, "Robotics for surgery," *Annu. Rev. Biomed. Eng*., 211–240 (1999).
11. T. C. Lueth, A. Albrecht, M. Demirtas, S. Zachow, E. Heissler, M. Klein, H. Menneking, G. Hommel and J. Bier, "A surgical robot system for maxillofacial surgery," *IEEE International Conference on Industrial Electronics, Control, and Instrumentation* (IECON) Aachen, Germany (1998) pp. 2470–2475.
12. J. M. Drake, M. Joy, A. Goldenberg and D. Kreindler, "Computer and robotic assisted resection of brain tumors," *Proceedings of 5th International Conference on Advanced Robotics*, Pisa, Italy (1991) pp. 888–892.
13. D. Glauser, P. Flury, N. Villotte and C. W. Burckhardt, "Conception of a robot dedicated to neurosurgical operations," *Proceedings of 5th International Conference on Advanced Robotics*, Pisa, Italy (1991), pp. 899–904.
14. J. Brief, H. Hassfeld, T. Redlich, C. Ziegler, J. Muenchenberg and S. Daueber, "Robot assisted insertion of dental implants—A clinical evaluation," *Proceedings of the Computer Assisted Radiology and Surgery*, San Francisco, USA (2000) pp. 932–937.
15. T. Lueth and J. Bier, "Robot Assisted Intervention in Surgery," **In:** *Neuronavigation-Neurosurgical and Computer Scientific Aspects* (J. M. Gilsbach and H. S. Stiehl eds.) (Springer-Verlag, 1999).
16. S. Kondo, Y. Okada, H. Iseki, T. Hori, K. Takakura, A. Kobayashi and H. Nagata, "Thermological study of drilling bone tissue with a high-speed drill," *Neurosurgery* **46**(5), 1162–1168 (May 2000).
17. G. Alici and R. Daniel; "Robotic drilling under force control: Execution of a task", *Proceedings of the 1993 IEEE/RSJ International Conference on Intelligent Robotics and Systems*, Yokohama, Japan (1993).
18. B. Allotta, G. Giacalone and L. Rinaldi; "A hand-held drilling tool for orthopedic surgery," *IEEE/ASME Trans. Mechatronics* **2**(4), (Dec. 1997).
19. P. Pott, H. Scharf and M. L. Schwarz, "Today's state of the art in surgical robotics," *Comput. Aided Surg.* **10**(2), 101–132 (Mar. 2005).
20. K. Cleary, V. Watson, D. Lindisch, R. Taylor, G. Fichtinger, S. Xu, C. White, J. Donlon, M. Taylor, A. Patriciu, D. Mazilu and D. Stoianovici, "Precision placement of instruments for minimally invasive procedures using a "Needle Driver" robot," *Int. J. Med. Robot. Comput. Assisted Surg.* **1**(2), 40–47 (Jan. 2005).
21. K. Cleary, K. Zigmundb, B. Banovaca, F. Whitec and D. Stoianovici, "Robotically assisted lung biopsy under CT fluoroscopy: Lung cancer screening and phantom study," *Proceedings of Computer Assisted Radiology and Surgery*, Berlin, Germany (2005) pp. 740–745.
22. S. D. Chang, "The cyberknife: Potential in patients with cranial and spinal tumors", *Am. J. Cancer* **4**(6), 383–393 (2005).
23. D. Stoyanov, A. Darzi and G. Z. Yang, "A practical approach towards accurate dense 3D depth recovery for robotic laparoscopic surgery", *Comput. Aided Surg.* **10**(4), 199–208 (Jul. 2005).

https://doi.org/10.1017/S0263574706003195 Published online by Cambridge University Press